ARTICLE

Arf6 regulates RhoB subcellular localization to control cancer cell invasion

Kossay Zaoui[1,2], Charles V. Rajadurai[1,2] (ID), Stéphanie Duhamel[2] (ID), and Morag Park[1,2,3,4] (ID)

The ADP-ribosylation factor 6 (Arf6) is a small GTPase that regulates endocytic recycling processes in concert with various effectors. Arf6 controls cytoskeletal organization and membrane trafficking; however, the detailed mechanisms of regulation remain poorly understood. Here, we report that Arf6 forms a complex with RhoB. The interaction between RhoB and Arf6 is mediated by the GCI (glycine, cysteine, and isoleucine) residues (188–190) of RhoB. Specific targeting of Arf6 to plasma membrane or mitochondrial membranes promotes recruitment and colocalization of RhoB to these membrane microdomains. Arf6 depletion promotes the loss of RhoB from endosomal membranes and leads to RhoB degradation through an endolysosomal pathway. This results in defective actin and focal adhesion dynamics and increased 3D cell migration upon activation of the Met receptor tyrosine kinase. Our findings identify a novel regulatory mechanism for RhoB localization and stability by Arf6 and establish the strict requirement of Arf6 for RhoB-specific subcellular targeting to endosomes and biological functions.

Introduction

The Met receptor tyrosine kinase (RTK) plays a crucial role in cell motility during embryonic development, wound healing, and tissue homeostasis. In response to its ligand, hepatocyte growth factor (HGF), Met coordinates the dynamic polarization of cells by regulating formation of cell protrusions, actin cytoskeleton remodeling, and formation and turnover of focal adhesions (FAs; Gherardi et al., 2012). Dysregulated Met signaling contributes to tumor progression by promoting tumor cell survival, as well as cell migration and invasion (Lai et al., 2009). However, the mechanisms through which Met regulates cell motility and cytoskeleton dynamics remain poorly understood.

Arf6, the least conserved member of the Arf family of GTPases, belongs to the Ras GTPase superfamily and localizes to the plasma membrane (PM) and endosomal compartments (D'Souza-Schorey and Chavrier, 2006). Arf6 is activated downstream from Met (Palacios and D'Souza-Schorey, 2003; Miura et al., 2017) and regulates endocytic membrane trafficking (Gillingham and Munro, 2007; Grossmann et al., 2019), including the Met RTK (Parachoniak et al., 2011). Arf6 also regulates the remodeling of actin cytoskeleton and FA dynamics to control cell motility (D'Souza-Schorey et al., 1997; Radhakrishna and Donaldson, 1997; Matsumoto et al., 2017). One role for Arf6 in cell migration is mediated through the regulation of members of the Rho family of small GTPases, either Rac1 (Boshans et al., 2000; Cotton et al., 2007) or Cdc42 (Osmani et al., 2010). However, the detailed mechanisms for Arf6 influence on cell motility downstream from Met remain elusive.

Rho GTPases are crucial regulators of the actin cytoskeleton rearrangements and FA dynamics (Ridley et al., 2003). They function as molecular switches and interact with downstream effector molecules to propagate the signal transduction in their GTP-loaded state (Bourne et al., 1991). They are required for effective cell migration and invasion (Ridley et al., 2003) as well as cell proliferation, apoptosis, and mitosis (Spiering and Hodgson, 2011). Although there are >20 human Rho GTPases, only a few have been studied downstream of Met despite their involvement in cell migration. To date, a role for Rac1, Cdc42, and RhoA in regulating cell migration downstream from Met has been identified (Takaishi et al., 1994; Royal et al., 2000; Lamorte et al., 2002), but involvement of other members, such as RhoB, has not been established.

The Rho family of GTPases includes the three isoforms RhoA, RhoB, and RhoC, which are 85% identical in sequence, with most differences concentrated in the C-terminus. Prenylation at the C-terminus is crucial for their function in cell growth, oncogenic transformation, and cytoskeleton organization, as well as their localization and stability (Wheeler and Ridley, 2004). Rho GTPases are generally localized in the cytoplasm and, in

[1]Department of Biochemistry, McGill University, Montreal, Quebec, Canada;   [2]Rosalind and Morris Goodman Cancer Centre, McGill University, Montreal, Quebec, Canada; [3]Department of Medicine, McGill University, Montreal, Quebec, Canada;   [4]Department of Oncology, McGill University, Montreal, Quebec, Canada.

Correspondence to Morag Park: morag.park@mcgill.ca;   Stéphanie Duhamel: stephanie.duhamel@mcgill.ca.

response to stimuli, translocate to the PM. Notably, RhoB is also present in the endosomes (Mellor et al., 1998; Wheeler and Ridley, 2004; Wherlock et al., 2004; Rondanino et al., 2007), multivesicular bodies, and nucleus (Ju and Gilkes, 2018). RhoB has been implicated in the regulation of epidermal growth factor receptor and platelet-derived growth factor receptor-β trafficking and signaling (Adamson et al., 1992; Robertson et al., 1995; Gampel et al., 1999; Huang et al., 2007). RhoB depletion promotes cell migration (Vega et al., 2012; Tseliou et al., 2016; Vega and Ridley, 2018) and membrane ruffling but impairs cell spreading and lamellipodium extension (Vega et al., 2012). Mechanical details of RhoB retention at the endosomal membrane and consequent effect on cell migration remain poorly understood. Here, we establish that Arf6 forms a complex with RhoB, and the deletion of the tripeptide sequence GCI (glycine, cysteine, and isoleucine; 188–190), specific to RhoB and absent in RhoA, disrupts its interaction with Arf6 and its localization to the endosomes. Our findings identify a novel regulatory mechanism for RhoB localization and stability by Arf6. Moreover, we found that Arf6 is necessary for specific subcellular targeting of RhoB to endosomes and, thus, the regulation of membrane trafficking and cell motility.

Results

The ability of Arf6 to regulate actin cytoskeleton remodeling is central to its role in cell migration and tumor invasion (Gillingham and Munro, 2007; Yamauchi et al., 2017). Arf6 is activated in response to HGF and modulates Met recycling as well as Met-dependent morphogenic events in polarized epithelia (Palacios and D'Souza-Schorey, 2003; Parachoniak et al., 2011). However, its role in actin cytoskeletal remodeling and FA dynamics in nonpolarized tumor cells following Met activation remains unknown. To address this, we examined the effect of Arf6 depletion by RNAi in cancer cells (HeLa) in response to HGF. Depletion of Arf6 with siRNA-mediated knockdown (KD) in HeLa cells reduced cell spreading but induced long projections in 80% of adherent cells (5 µm in control cells compared with 10 µm in Arf6 KD cells; Fig. 1, A and B; and Fig. S1, A and B). After HGF stimulation, Arf6 KD cells failed to form large lamellipodial extensions as observed in control cells yet formed enhanced projections in 88% of adherent cells, which ranged from 12 µm in control cells to 25 µm in Arf6 KD cells (Fig. 1, A and B; and Fig. S1, A and B). Video microscopy analysis revealed that the formation of long projections in Arf6 KD cells appeared at the rear of migrating cells (Fig. 1 B). Importantly, reexpression of RNAi-resistant Arf6 rescued this altered cell morphology (Fig. 1, A and B; and Fig. S1, A and B), highlighting the specificity and dependence of these responses to Arf6. Importantly, reexpression of RhoB did not restore morphology defects induced by Arf6 depletion. Moreover, Arf6 KD was sufficient to destabilize ectopic RhoB protein levels (Fig. 1, A and B). Together, these observations further support that Arf6 acts upstream of RhoB to control cancer cell morphology.

Such a dramatic change in cell morphology in response to Arf6 depletion could be a consequence of the known role of Arf6 in modulating activities of Rho family members RhoA, Rac1, and Cdc42, which regulate actin cytoskeleton and cell morphology (Boshans et al., 2000; Cotton et al., 2007; Osmani et al., 2010). To examine the requirement of Arf6 in actin cytoskeletal remodeling downstream of activated Met, we investigated the activation status of Rho family members. In response to HGF stimulation, the activation status of RhoA was not altered in Arf6 KD cells compared with control cells (Fig. 1 C). Similarly, HGF stimulation promoted RhoB activation (Fig. 1 D). However, unlike RhoA, Arf6 depletion dramatically decreased RhoB activity in response to HGF stimulation compared with control cells (Fig. 1 D). Moreover, a concomitant decrease in RhoB protein levels following Arf6 KD was observed regardless of HGF stimulation (Fig. 1 E), while RhoA and RhoC protein levels remained mostly unaltered (Figs. 1 F and S1 C). To further substantiate our observations, we performed immunofluorescence on endogenous RhoB and Arf6 in HGF-stimulated HeLa cells and showed that RhoB was not detectable by immunofluorescence in Arf6-depleted cells, while KD of RhoB did not affect Arf6 expression levels or localization (Fig. S1 D).

RhoB has been reported to be rapidly degraded through a lysosomal pathway (Engel et al., 1998; Pérez-Sala et al., 2009). To elucidate the involvement of Arf6 in RhoB turnover, Arf6 was depleted in HeLa cells pretreated with a v-ATPase inhibitor, bafilomycin A1. Bafilomycin A1 treatment stabilized RhoB protein levels following Arf6 KD and restored RhoB activation in response to HGF (Fig. 1, D and E). However, RhoA protein levels in Arf6 KD HeLa cells pretreated with bafilomycin A1 remained unaltered (Fig. 1 F). Hence, Arf6 KD does not alter the ability of Met to activate RhoB, but instead decreases the steady-state RhoB protein level.

To examine whether the altered cell morphology following Arf6 KD correlated with the observed decrease in RhoB protein, we depleted RhoB using RNAi. Notably, RhoB KD resulted in the formation of cells with multiple elongated tails in a similar manner to Arf6 KD (Fig. S1, E–G). This observation is consistent with previous studies where similar alterations in cell morphology were observed (Bousquet et al., 2009; Vega et al., 2012). However, no change in Arf6 GTPase activity was detected following RhoB depletion (Fig. S1 H). Hence, the generation of long protrusions observed in RhoB and Arf6 KD cells suggests that they may be involved in the same signaling pathway downstream from Met.

Arf6 localizes to the PM as well as endosomes, while RhoB is mainly found at endosomes (Radhakrishna and Donaldson, 1997; Wheeler and Ridley, 2004). To establish whether these proteins colocalize, we examined their subcellular localization in HeLa cells. Confocal microscopy analysis revealed that in the absence or presence of HGF, a portion of endogenous Arf6, colocalized with RhoB in intracellular vesicles at the cell periphery and perinuclear regions (Fig. 2, A and B). To determine whether RhoB localization to endosomal compartments was mediated through Arf6, the interaction between RhoB and Arf6 was investigated. We found that endogenous Arf6 coimmunoprecipitated with RhoB (Fig. 2 C). Interestingly, pull-down experiments revealed that neither Arf6 nor RhoB is required in their active GTP-bound form to interact (Fig. 2 D). Moreover, transient expression of WT Arf6 coimmunoprecipitated with RhoB in the
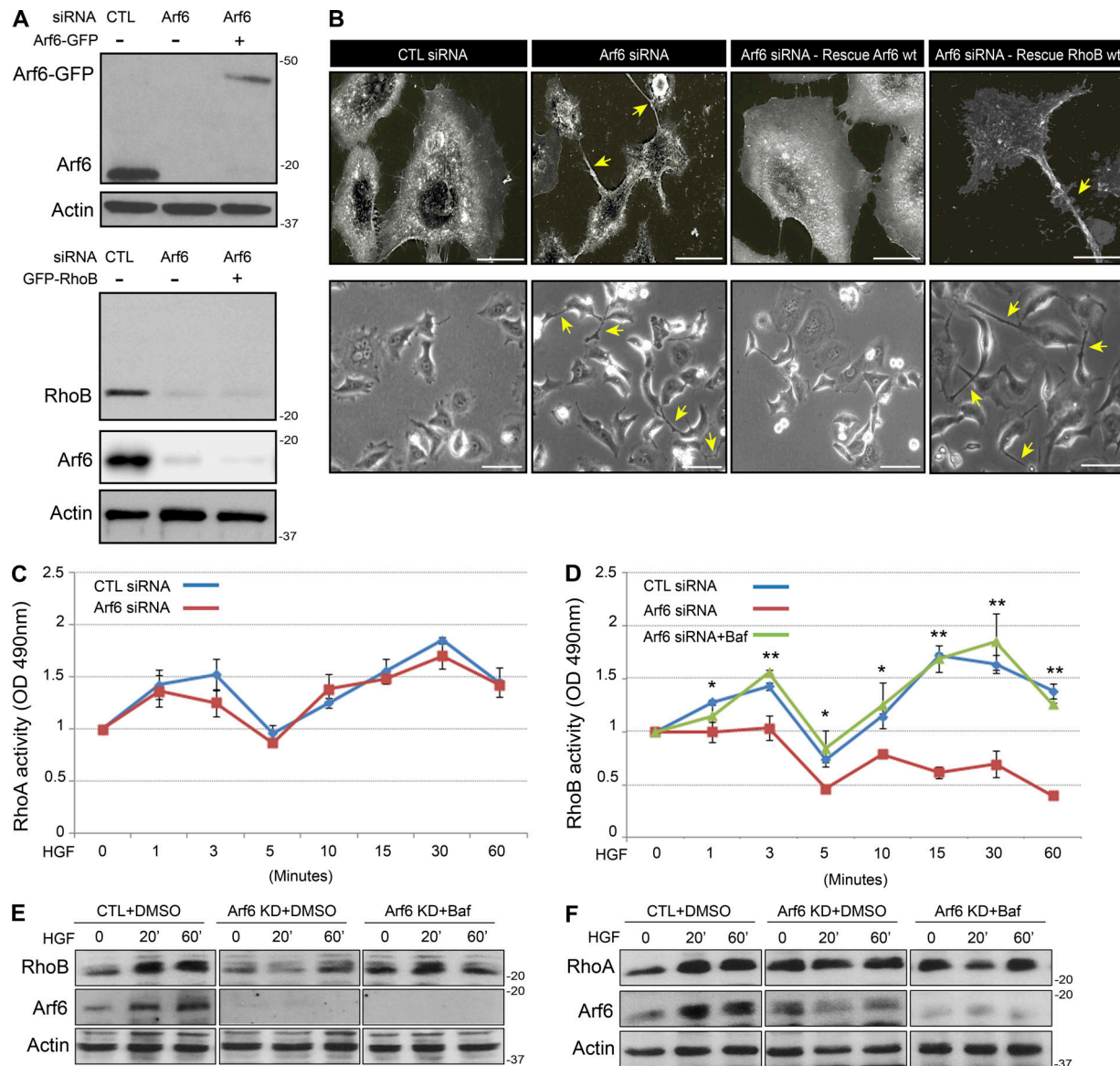
Figure 1. **Arf6 depletion dramatically alters cell morphology and reduces RhoB activity in response to HGF stimulation. (A)** Western blot of Arf6 KD and rescue levels in HeLa cells with the indicated constructs. CTL, control. **(B)** Scanning electron micrographs (scale bar = 30 µm) and live-cell images (scale bar = 10 µm) of HeLa cells transfected with control or Arf6 siRNAs and rescued with Arf6-GFP or GFP-RhoB, stimulated with 0.5 nM of HGF (20 min). Arrows indicate the tail of cells. **(C and D)** Active GTP-RhoA (C) and RhoB (D) were examined in HeLa cell lysates of control and Arf6 KD. HeLa cells were pretreated for 2 h with DMSO or 10 nM of bafilomycin A1 (Baf) and stimulated with HGF at different time points as indicated. **(E and F)** Western blot showing RhoB (E) and RhoA (F) protein levels. All quantified data indicate mean values ± SEM from three independent experiments. P values based on comparisons with control: *, $P < 0.05$; **, $P < 0.001$.

absence of HGF, suggesting that this interaction may be constitutive (Fig. 2 E). Consistent with this hypothesis, Arf6 mutants that adopted either a dominant-active (DA) conformation (Arf6-Q67L) or a dominant-negative (DN) conformation (Arf6-T27N) coimmunoprecipitated with RhoB. These results further indicate that Arf6 does not need to be GTP loaded to interact with RhoB. Similarly, reciprocal coimmunoprecipitations confirmed the ability of WT-RhoB, DA-RhoB (V14), and DN-RhoB (N19) to coimmunoprecipitate with Arf6, indicating that RhoB activation was not required for this interaction (Fig. 2 F). Although the amino acid sequences of RhoA and RhoB are 88% identical (Wheeler and Ridley, 2004), RhoA failed to

coimmunoprecipitate with Arf6 (Fig. S2 A), and RhoA localization to PM was not perturbed by Arf6 depletion (Fig. S2, B and C). To determine whether the interaction between Arf6 and RhoB is direct, we used far-Western analysis to examine the ability of WT-RhoB, DA-RhoB, DN-RhoB, and a known Arf6-binding partner, Golgi-localized γ-ear–containing Arf-binding protein 3 (GGA3), to interact with Arf6 purified from bacteria. As expected, Arf6 bound to GGA3. Interestingly, Arf6 was also associated with WT-RhoB, DA-RhoB, and DN-RhoB (Fig. 2 G). Similarly, in vitro binding assays with recombinant proteins confirmed the interaction of Arf6 with WT-RhoB, DA-RhoB, and DN-RhoB, suggesting that RhoB activity is not required
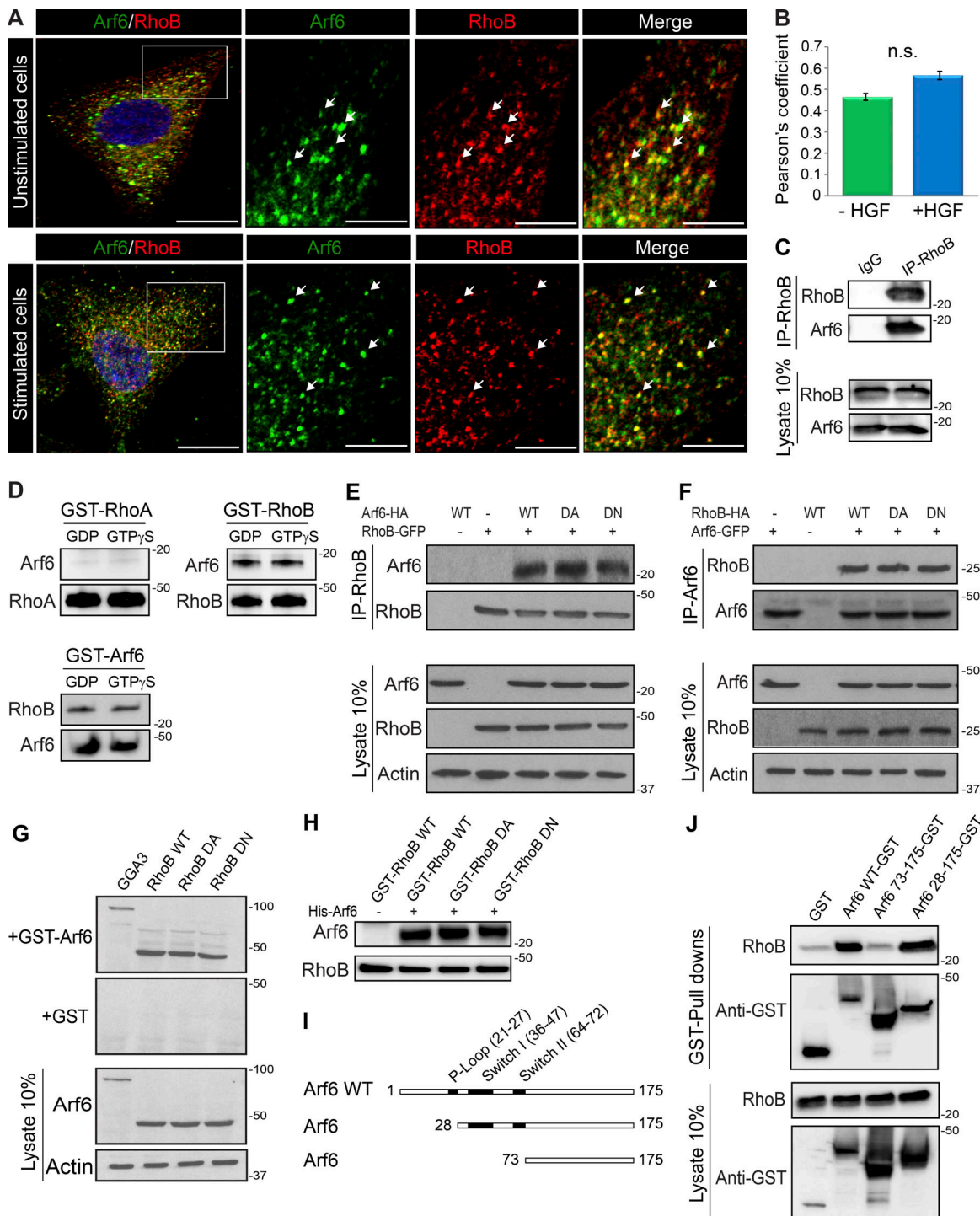
Figure 2. Arf6 directly interacts with RhoB and colocalizes to the same subcellular structures. (A) HeLa cells untreated or treated with 0.5 nM HGF (20 min) were stained for endogenous Arf6 and RhoB. Insets show enlarged region. Arrows indicate multiples vesicles positive for both Arf6 and RhoB. **(B)** Colocalization between Arf6 (green), RhoB (red), and DAPI (blue) was represented as Pearson's coefficient and measured for individual HeLa cells (*n* = 20). **(C)** Endogenous RhoB coprecipitated with endogenous Arf6 of HeLa cells, which were lysed and subjected to immunoprecipitation (IP) and analyzed by immunoblotting. **(D)** In vitro GST pull-down assay of purified RhoA or RhoB with purified Arf6, loaded with GDP or GTPγS. **(E)** HeLa cells were cotransfected with Arf6-HA (WT), Arf6-HA (DA), or Arf6-HA (DN); lysed; and subjected to IP with RhoB-GFP (WT) and Western blotted as shown. **(F)** HeLa cells were cotransfected with RhoB-HA (WT), RhoB-HA (DA), and RhoB-HA (DN), lysed, and subjected to IP with Arf6-GFP (WT) and Western blotted as shown. **(G)** HeLa cells transfected with GFP-RhoB (WT), GFP-RhoB (DA), GFP-RhoB (DN), or GFP-GGA3 were lysed and subjected to IP with an anti-GFP antibody; protein complexes were separated by SDS-PAGE and transferred to nitrocellulose membranes. The membranes were incubated with fusion protein GST alone or GST-Arf6 and immunoblotted. **(H)** In vitro binding assay with purified recombinant proteins. GST-RhoB (WT), GST-RhoB (DA), or GST-RhoB (DN) in the presence or absence of His-Arf6, subjected to a GST pull-down and Western blot as shown. **(I)** Schematic of Arf6 mutant constructs. **(J)** GST, GST-Arf6, GST-Arf6 28–175, and GST-Arf6 73–175 were transfected into HeLa cells. Protein lysates were then subjected to a GST pull-down and immunoblotted for endogenous RhoB. All quantified data indicate mean values ± SEM from three independent experiments. Scale bar = 10 μm; 5 μm for magnification. P values based on comparisons with control: n.s., nonsignificant.

(Fig. 2 H). Additional in vitro binding experiments with Arf6 deletion mutants showed that the domain containing amino acids 28–73 was critical for Arf6 interaction with RhoB (Fig. 2, I and J). Taken together, these data demonstrate a previously undescribed direct interaction between Arf6 and RhoB.

The activities of Arf6 at the PM are complex, and Arf6 is likely activated and inactivated at many locations along the PM, where it can influence the sorting of membrane proteins, endocytic pathways, and the structure of the PM (Donaldson, 2003). Here we observed that Arf6 and RhoB predominantly colocalize at endocytic vesicles in HeLa cells (Fig. 2, A and B). Given that Arf6 forms a complex with RhoB, we hypothesized that Arf6 could retain RhoB in Arf6-positive vesicles, allowing spatially restricted activation of RhoB. To explore whether Arf6 actively promotes RhoB recruitment to the endosomal membranes, we expressed a fusion protein (Mito-Arf6-EGFP) to target Arf6 to the mitochondria in SKBr3 cells and, in parallel, used MitoTracker to stain mitochondria in living cells (Fig. S2 D). Whereas TagRFP-T-RhoB failed to localize with mitochondria when coexpressed with a control Mito-EGFP fusion protein (Fig. S2 D), the TagRFP-T-RhoB localized to mitochondria following coexpression with Mito-Arf6-EGFP (Fig. S2 E). Importantly, under these conditions, RhoA remained localized to the PM and in membrane ruffles, which is consistent with its inability to bind Arf6 (Fig. S2, A and E). To further validate the role of Arf6 in regulating RhoB subcellular localization and stability, we investigated whether targeting Arf6 to the PM by expressing a fusion protein (Myr-Arf6-GFP) was sufficient to recruit RhoB to the PM. In agreement, TagRFP-T-RhoB accumulated constitutively to the PM and in membrane ruffles in cells expressing Myr-Arf6-GFP, regardless of Met activation, whereas TagRFP-T-RhoB did not colocalize with EGFP in control cells, confirming the specificity of recruitment to the PM and ruffles (Fig. S2 F). Our results were then confirmed by immunostaining of endogenous RhoB, which localized to the PM in cells expressing Myr-Arf6-GFP (Fig. S2 G). Taken together, these results support a role for Arf6 in recruiting RhoB to specific subcellular compartments, including plasma and endosomal membranes.

Arf6 interacts with RhoB but not with RhoA (Fig. 2, C and D; and Fig. S2 A), suggesting that the C-terminus of RhoB contains specific sequences that may be responsible for its interaction with Arf6. To test this hypothesis, we generated multiple RhoB mutants and attempted coimmunoprecipitations with Arf6 (Fig. 3 A). We found that the isoprenylation-deficient mutants of RhoB (RhoB-C193S, RhoBΔNCCKVL, and RhoBΔKRYGSQN) efficiently bound Arf6. However, the deletion of the last 17 residues in the C-terminus of RhoB (RhoBΔ17) disrupted its interaction with Arf6 (Fig. 3, A–C). The C-terminus of RhoB contains a tripeptide GCI, localized at the residues 188–190. This tripeptide GCI is a unique feature of RhoB and is not found in any other known protein or Rho GTPase (Wang and Sebti, 2005; Vega and Ridley, 2018). Therefore, we hypothesized that the GCI tripeptide may be important for Arf6–RhoB complex formation. To test this possibility, we generated deletion constructs of RhoB lacking either individual amino acids of GCI residues or lacking all three GCI residues (RhoBΔGCI, RhoBΔG188, RhoBΔC189, and RhoBΔI190). Surprisingly, none of these

mutants coimmunoprecipitated with Arf6 (Fig. 3 C). To confirm the requirement of the GCI peptide for the interaction with Arf6, we generated a mutant of RhoA containing the GCI residues (RhoA-GCI), where GCI amino acids were added at the corresponding position (188-189-190) to mimic the sequence of WT RhoB. We found that RhoA-GCI coimmunoprecipitated with Arf6 (Fig. 3 D), suggesting that the GCI residues are important to mediate the interaction with Arf6. As palmitoylation of the cysteine 189, part of the GCI motif, is required for RhoB subcellular localization and protein stability (Pérez-Sala et al., 2009), we sought to determine whether palmitoylation was required for Arf6 interaction. We found that ectopic expression of Arf6-GFP in HeLa cells did not alter RhoB palmitoylation (Fig. 3 E). Immunoprecipitation of Arf6 in the presence of a general palmitoylation inhibitor, 2-bromopalmitate (2-BP), which inhibits palmitic acid biosynthesis and thereby indirectly inhibits protein palmitoylation, revealed that RhoB palmitoylation was not required for interaction with Arf6. Moreover, inhibition of palmitoylation appeared to increase RhoB–Arf6 complex formation (Fig. 3 F).

We next expressed RhoB mutants (RhoBΔ17, RhoBΔGCI, RhoBΔG188, RhoBΔC189, RhoBΔI190, RhoBΔG193S, RhoBΔNCCKVL, and RhoBΔKRYGSQN) in SKBr3 cells and examined their subcellular localization by time-lapse microscopy. Consistent with the immunoprecipitation results, the RhoB mutants (RhoBΔ17, RhoBΔGCI, RhoBΔG188, RhoBΔC189, and RhoBΔI190) failed to localize to the endosomal membranes (Fig. 3 G). Furthermore, the RhoA mutant containing the GCI residues (RhoA-GCI) accumulated at the endosomes, whereas WT RhoA localized to the cytoplasm and the PM ruffles (Fig. 3 G). Taken together, these results suggest that the RhoB GCI residues in the context of our study are important for RhoB interaction with Arf6 and its association with endosomes.

Following HGF stimulation, Met is internalized into the endosomal trafficking network (Fig. S3 A). This was confirmed using Alexa Fluor 555–labeled HGF, where internalized HGF/Met complexes entered into RhoB-GFP positive endosomes at 20 min after stimulation (Fig. S3 B). Hence, these observations provide a model through which a Met-dependent signal could activate RhoB in a spatially restricted manner.

RhoB has been shown to induce stress fiber formation when overexpressed (Wheeler and Ridley, 2004). Since actin stress fibers contribute to changes in the cell shape and are involved in tail retraction during cell migration (Pellegrin and Mellor, 2007), we investigated whether actin organization is altered in Arf6-depleted cells. In response to HGF stimulation, actin-mCherry localized within actin stress fibers and in developing lamellipodia in control cells (Fig. 4 A). In contrast, 83% of Arf6 KD cells, 80% of RhoB KD cells, and 74% of the cells expressing RhoBΔGCI elicited a decreased localization of actin-mCherry to stress fibers. Furthermore, stress fibers appeared thinner under these conditions than in control cells. The number of stress fibers at the leading edge was decreased in both Arf6- and RhoB-depleted cells (65% in Arf6 and RhoB KD cells and 75% in cells expressing RhoBΔGCI), indicating that the formation of actin stress fibers was perturbed (Fig. 4, B and C). However, in opposition to WT-Arf6 or WT-RhoB, expression of RhoBΔGCI did not restore this phenotype (Fig. 4, A–C).
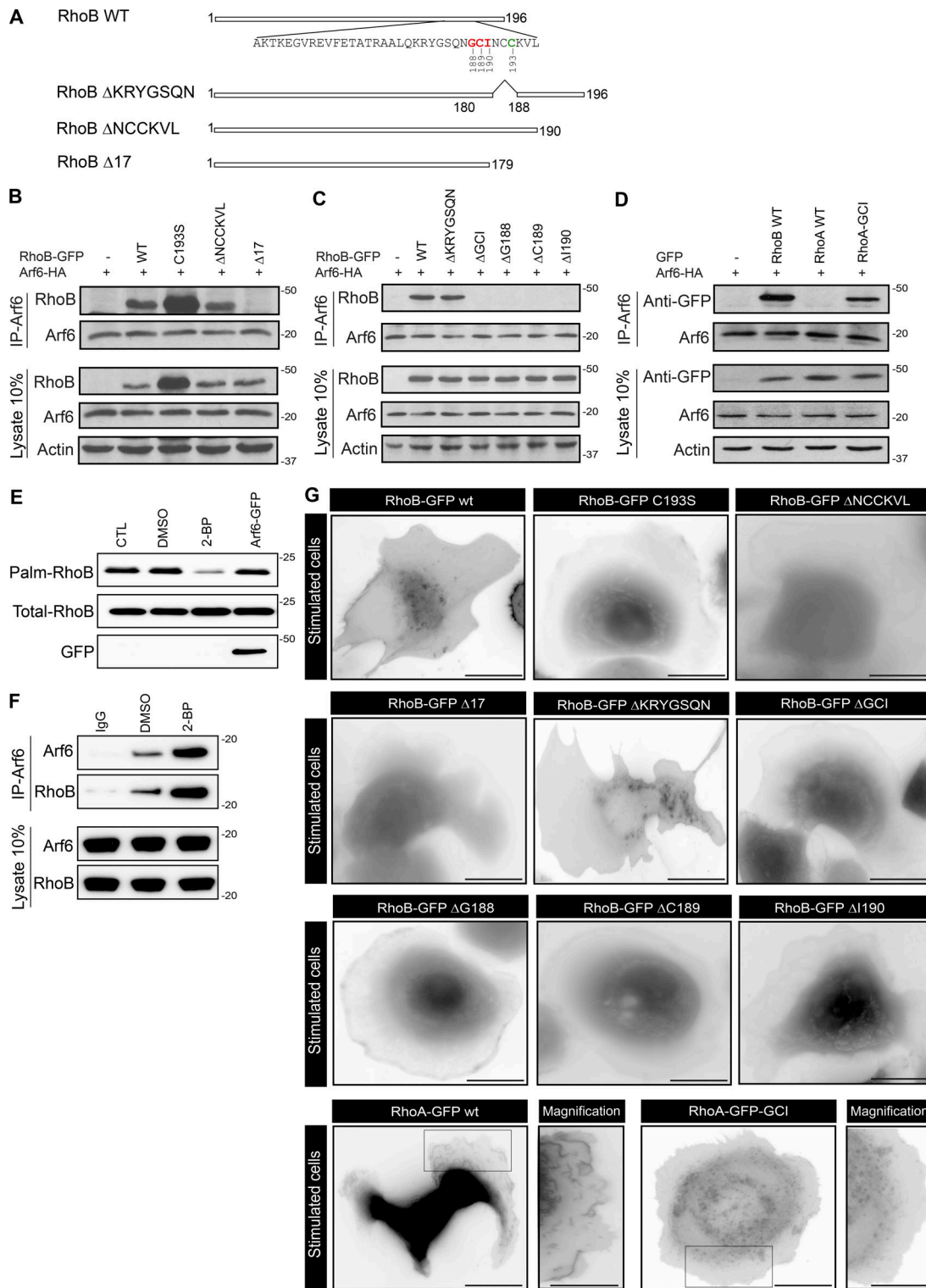
Figure 3. **The GCI tripeptide of RhoB mediates its interaction with Arf6. (A)** Schematic of RhoB mutant constructs. **(B)** HeLa cells were cotransfected with Arf6-HA (WT) and RhoB-GFP (WT), RhoB-GFP (C193S), RhoB-GFP (ΔNCCKVL), or RhoB-GFP (Δ17); lysed; and subjected to immunoprecipitation (IP) using an anti-HA antibody and blotted as shown. **(C)** HeLa cells were cotransfected with RhoB-GFP (WT), RhoB-GFP (ΔKRYGSQN), RhoB-GFP (ΔGCI), RhoB-GFP (ΔG188), RhoB-GFP (ΔC189), or RhoB-GFP (ΔI190) and then subjected to IP with Arf6-HA (WT) and blotted as shown. **(D)** HeLa cells were cotransfected with RhoB-GFP (WT), RhoA-GFP (WT), or RhoA-GFP (GCI) and then subjected to IP with Arf6-HA (WT) and blotted as shown. **(E)** Level of palmitoylated RhoB in the presence of the palmitoylation inhibitor, 2-BP (100 μM, 2 h), or ectopically expressed Arf6-GFP in HeLa cells. CTL, control. **(F)** IP of endogenous Arf6 in HeLa cells treated with DMSO or 2-BP and blotted as shown. **(G)** SKBr3 cells were transfected with RhoB mutants as indicated and stimulated with HGF (20 min). Insets show enlargement of the cell leading edge. Representative images of three independent experiments. Scale bar = 10 μm; 5 μm for magnification.
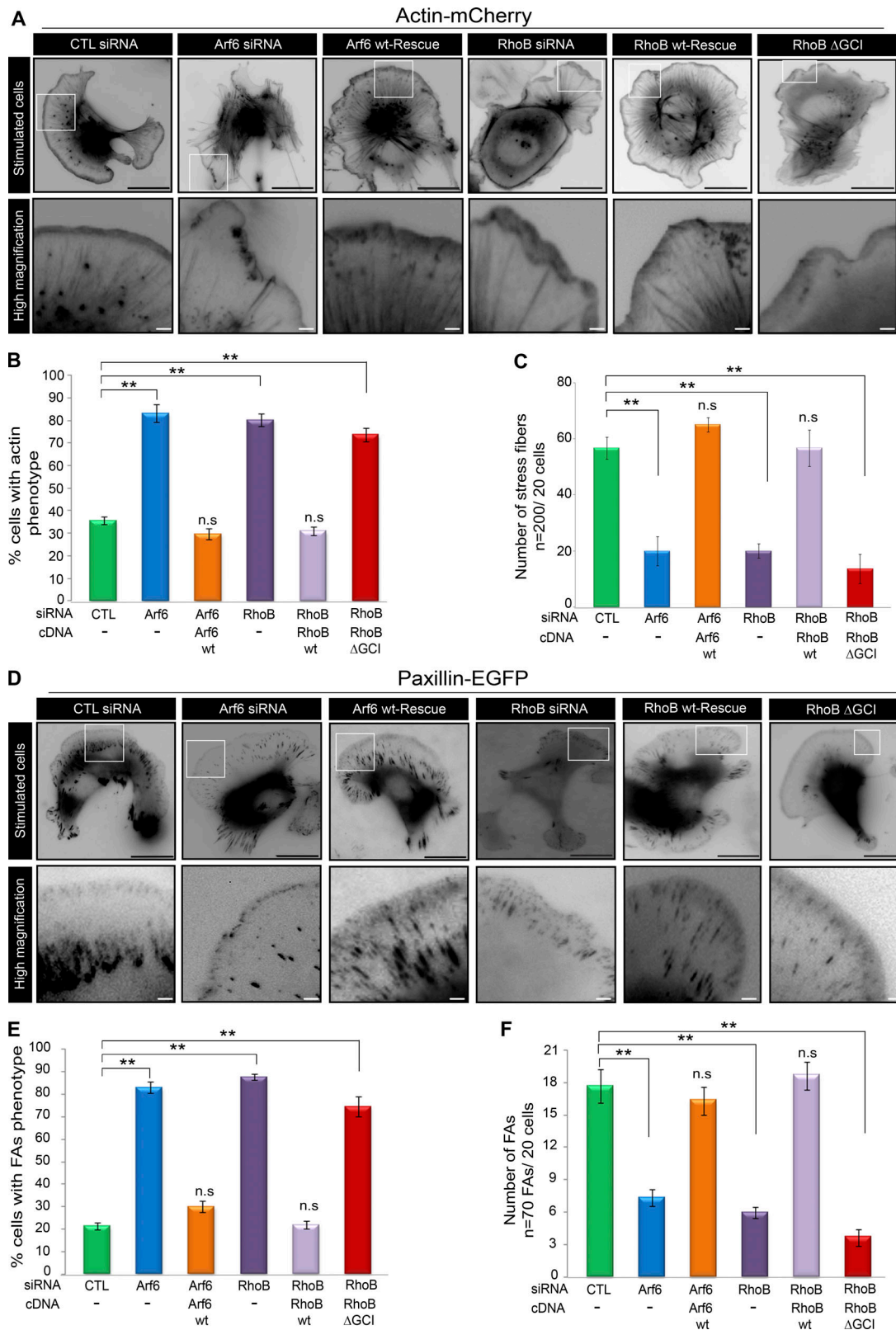
Figure 4. **Either depletion of Arf6 or RhoB or expression of RhoBΔGCI regulates actin stress fibers and FA dynamics. (A)** SKBr3 cells cotransfected with actin-mCherry and RhoB/Arf6 siRNAs or Arf6/RhoB/RhoBΔGCI were stimulated with 0.5 nM HGF (20 min). Insets show enlarged region from the cell leading edge. CTL, control. **(B)** Percentage of cells with reduced actin cables were scored. **(C)** Number of fluorescence peaks representing stress fibers in SKBr3 cells from A are shown. **(D)** SKBr3 cells cotransfected with Paxillin-EGFP and RhoB/Arf6 siRNAs or Arf6/RhoB/RhoBΔGCI cDNAs were stimulated with 0.5 nM HGF (20 min). Insets show enlarged region from the cell leading edge. **(E and F)** Percentage of cells with small FAs (E) and number of FAs (F) were scored. All quantified data indicate mean values ± SEM from three independent experiments. Scale bar = 10 µm; 2 µm for magnification. P values based on comparisons with control: n.s., nonsignificant; **, P < 0.001.

Zaoui et al.
Arf6 regulates RhoB to control cell invasion

Journal of Cell Biology
3818
https://doi.org/10.1083/jcb.201806111

Since FAs link actin stress fibers to the extracellular matrix and both Arf and Rho proteins regulate cell adhesions by enhancing actomyosin contractility (Riento and Ridley, 2003), we studied the FA dynamics. Using Paxillin as a marker of nascent and mature adhesions, we observed a striking decrease in the number and length of FAs in 83% of Arf6 KD cells, 88% of RhoB KD cells, and 75% of cells expressing RhoBΔGCI (Fig. 4, D–F; and Fig. 5 A). In accordance with the known role of actin stress fibers on FA turnover (Pellegrin and Mellor, 2007), the half-life of FAs was decreased at the leading edge (~12 min in control cell vs. ~9 min in Arf6 KD cells; ~12 min in control cell vs. ~7 min in RhoB KD cells; ~12 min in control cell vs. ~8 min in cells expressing RhoBΔGCI) but increased in the trailing edge of Arf6 KD cells in response to HGF (~15 min in control cell vs. ~21 min in Arf6 KD cells; ~15 min in control cell vs. ~22 min in RhoB KD cells; ~15 min in control cell vs. ~24 min in cells expressing RhoBΔGCI; Fig. 5 B). A similar change in actin stress fibers and FA number and length were observed for Arf6 KD or RhoB KD or expression of RhoBΔGCI, as shown by endogenous actin and Paxillin immunofluorescence (Fig. S3 C). Hence, we conclude that RhoB depletion promotes a similar decrease in actin stress fiber formation and FAs, as observed following Arf6 depletion. Importantly, expression of RhoB lacking CGI residues did not rescue this phenotype.

Several studies have implicated Arf6 and RhoB in the recycling and delivery of integrins to the PM via their actions on endosomal trafficking (Liu et al., 2001; Sabe, 2003; Wheeler and Ridley, 2007). Thus, regulation of certain components required for FA stability may be orchestrated by Arf6-RhoB signaling. To establish if Arf6 regulates the dynamic properties of FAs necessary for cell rear retraction and migration, we performed FRAP on cells expressing Paxillin-EGFP after 20 min of HGF stimulation. We found a significant difference in the fast recovery of FAs at the leading edge of migrating cells, as demonstrated by rapid diffusion of exogenously expressed Paxillin-EGFP to the bleached region in Arf6- or RhoB-depleted cells and in RhoBΔGCI-expressing cells, compared with control cells. Paxillin-EGFP fluorescence was reestablished in FAs in Arf6 KD cells by ~80 s after bleaching with 77% recovery, 75 s in RhoB KD cells with 69% recovery, and 70 s in cells expressing RhoBΔGCI with 71% recovery, compared with 108 s in control cells with 52% recovery (Fig. 5, C and D). No significant differences were observed in unstimulated cells (Fig. S3, D and E). Notably, HGF stimulation increased the percentage and rate recovery when compared with control conditions. These differences reflect the changes in FA dynamics after Arf6 or RhoB depletion or the impact of Arf6-RhoB dissociation following the expression of RhoBΔGCI. Taken together, these results support a role for the Arf6–RhoB complex in coordinating actin stress fiber assembly, FA turnover, and rear retraction.

Arf6 and RhoB are central components of the regulatory machinery that controls cell migration and invasion (Palacios et al., 2001; Vega et al., 2012). To determine whether the depletion of Arf6 or RhoB or the expression of RhoBΔGCI can affect cell invasion and dispersion following HGF stimulation, we used the highly invasive breast cancer cell line MDA-MB-231, which forms spheroid-like structures when embedded and cultured in 3D Geltrex matrix (Lee et al., 2007). While MDA-MB-231 control cells formed spheroid-like structures, Arf6 and RhoB depletion or the expression of RhoBΔGCI strongly altered the morphology of these spheroid-like structures (Fig. 5 E; Fig. S3, F and G; and Videos 1 and 2). The cells formed an elongated linear extension associated with a higher capacity to invade the matrix as single rounded cells (Fig. 5 E). Moreover, we found that Arf6 or RhoB depletion enhanced Met-dependent 3D cell migration. The migrated distance and migration speed under these conditions were consistently increased. Interestingly, the reintroduction of RhoBΔGCI in RhoB KD cells, as well as RhoB WT in Arf6 KD cells, was not sufficient to reduce the increased cell migration induced by Arf6 depletion (Fig. 5, E–G). Taken together, these results reveal the requirement of tripeptide sequence GCI of RhoB for efficient cell migration and invasion.

Discussion

The molecular mechanisms by which Arf6 or RhoB regulates cell migration remain elusive (Cotton et al., 2007; Bousquet et al., 2009; Vega et al., 2012). RhoB loss is mostly associated with increased cell motility (Bousquet et al., 2009; Vega and Ridley, 2018) and tumor progression in many cancer types such as lung, brain, ovarian, bladder, colorectal, gastric, and breast (Mazieres et al., 2004; Chen et al., 2016; Ju and Gilkes, 2018). However, a few studies suggest that RhoB may play two distinct and opposing roles in the context of tumor initiation versus tumor progression and aggressiveness (Kazerounian et al., 2013; Meyer et al., 2014). For example, in breast tumorigenesis, RhoB can act as a tumor suppressor by restricting epidermal growth factor receptor at the cell surface, thus impairing Akt signaling. But, after activation of the angiogenic switch, RhoB functions as a tumor promoter by sustaining endothelial Akt signaling, growth, and survival of stromal endothelial cells to mediate tumor angiogenesis (Kazerounian et al., 2013). In epithelial cells, the motile and invasive phenotype induced by the inhibition of RhoB is the result of the cytoskeletal alteration, leading to increased actin stress fibers, the loss of cell adhesion, and increased expression of the mesenchymal marker, vimentin (Bousquet et al., 2009).

Likewise, the effect of Arf6 on cell migration is under debate, since the results from various groups are contradictory, and Arf6 depletion has been linked to both increased and decreased cell motility (Cotton et al., 2007; Morishige et al., 2008; Hu et al., 2009; Li et al., 2009; Muralidharan-Chari et al., 2009; Grossmann et al., 2013). Under certain circumstances, the loss of Arf6 can lead to increased cell membrane ruffling and enhanced cell migration (Bousquet et al., 2009; Vega et al., 2012; Yoo et al., 2016). The lincRNA-RoR/miR-145/ARF6 pathway was shown to dysregulate E-cadherin localization and reduce cell–cell adhesion to promote cell invasion in triple-negative breast cancer cell lines. Arf6 is overexpressed in tumor and lymph node metastasis of triple-negative breast cancer (Eades et al., 2015), and high Arf6 expression is correlated with metastasis occurrence in pancreatic and lung cancers, as well as renal and squamous cell carcinomas (Hashimoto et al., 2016; Otsuka et al., 2016; Li et al., 2017). Therefore, the role of Arf6 and RhoB in cell motility
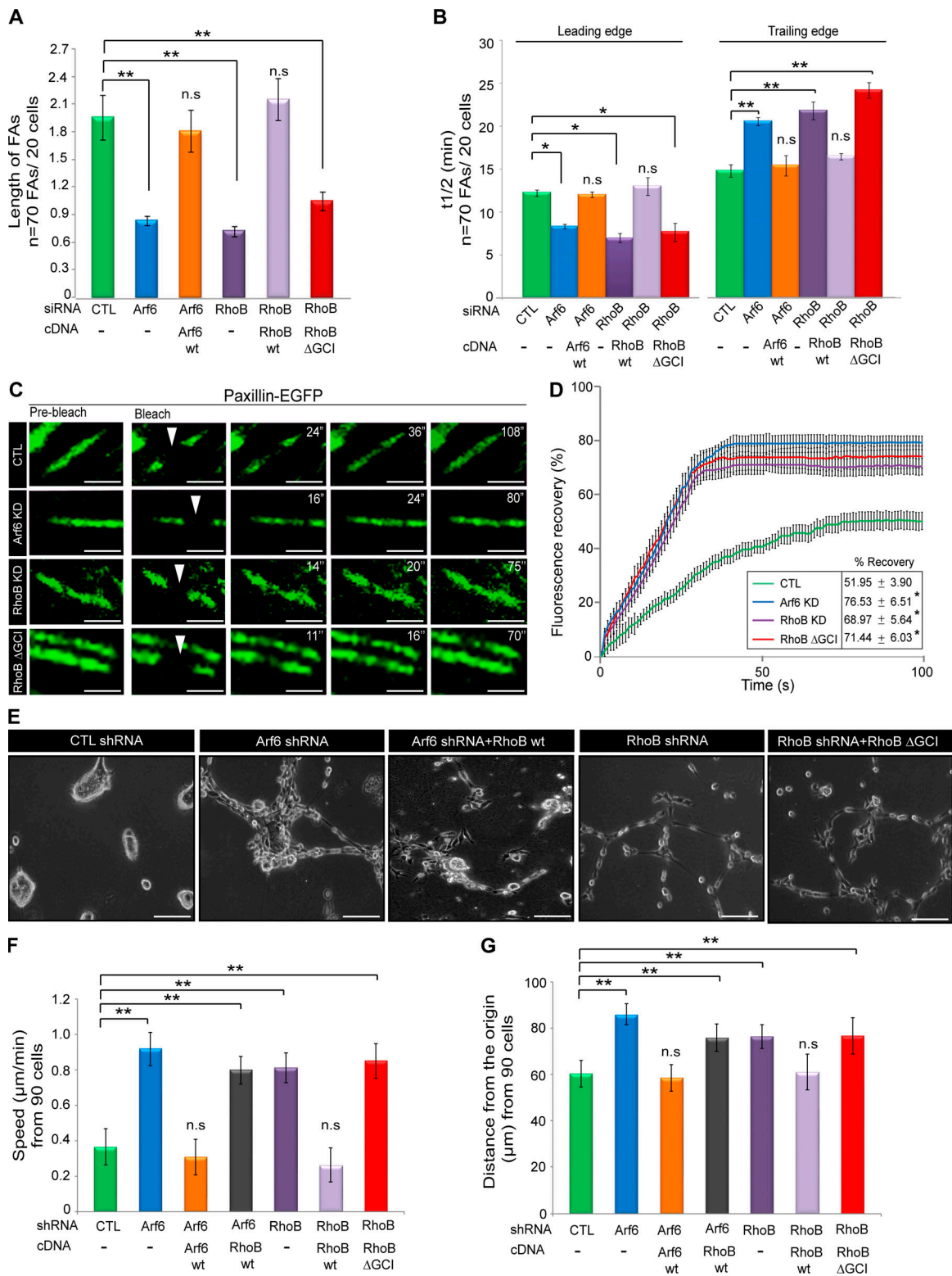
Figure 5. **The tripeptide sequence GCI of RhoB is critical for cell motility. (A and B)** Quantification of length (A) and half-life (B) of FAs was scored from transfected SKBr3 cells after HGF stimulation (20 min). CTL, control. **(C)** Fluorescence was bleached (arrowheads) within the stable FAs of control, Arf6 KD, RhoB KD, or RhoBΔGCI at the leading edge of migrating SKBr3 cells, and fluorescence recovery was monitored over time. **(D)** Quantification of Paxillin-EGFP fluorescence over time and percentage of recovery (box) are presented for Arf6 KD, RhoB KD, or RhoBΔGCI cells. **(E)** Phase-contrast images of HGF-treated MDA-MB-231 cells on collagen/Geltrex matrix transduced with Arf6 or RhoB shRNAs and rescued by RhoB WT or RhoBΔGCI. **(F and G)** Quantification of the speed (F) and distance from the origin (G) of MDA-MB-231 cells transduced with shRNAs and transfected with cDNAs as indicated, cultured on collagen/Geltrex matrix and stimulated with HGF. The distance from the origin was determined as the net displacement between the initial position and the final position observed during an 8-h period. All quantified data indicate mean values ± SEM from three independent experiments. Scale bar = 10 μm; 2 μm for magnification. P values based on comparisons with control: n.s., nonsignificant. *, P < 0.05; **, P < 0.001.

appears to be dependent on cell type and context, probably because they can affect both intracellular protein trafficking and actin organization. Here, we report that either depletion of Arf6 or RhoB or expression of RhoBΔGCI is sufficient to alter actin stress fibers and FA dynamics, leading to 3D cell invasion. Importantly, our findings extend the role of Arf6 to the regulation of RhoB-specific subcellular targeting to endosomes, stability, and biological functions.

Arf6 is a critical mediator of endocytosis and the recycling of multiple membrane receptors, such as G protein–coupled receptors and cadherin–catenin complexes (D'Souza-Schorey and Stahl, 1995; Palacios et al., 2001; Hunzicker-Dunn et al., 2002; Chen et al., 2003). Our study provides a detailed understanding at the molecular level of the regulation of RhoB stability and localization to endosomes via Arf6 GTPase. By controlling RhoB localization, Arf6 emerges as a crucial regulator of cell motility. Rho GTPases have polybasic regions upstream from their CAAX motif. However, the function of the secondary endosome membrane–targeting motif has remained largely unexplored (Michaelson et al., 2001).

The fact that Arf6 controls the spatiotemporal localization of RhoB supports a role for Arf6 as a "second signal" for RhoB engagement to endosomes in addition to the CAAX motif. Our observations highlight the importance of RhoB residues 188–190 (GCI) for interaction with Arf6 and subsequent activities. RhoB is palmitoylated at cysteine 189, and mutation of this site is sufficient to impair its targeting to the PM and enhance its stability. Similarly, palmitoylation of the C-terminal sequence of RhoB (CINCCKVL) is required for its rapid degradation by the lysosomal pathway (Pérez-Sala et al., 2009). Here, we found that palmitoylation inhibition using the 2-BP inhibitor enhanced RhoB–Arf6 complex formation (Fig. 3 F). This increase of Arf6–RhoB interaction may be a consequence of the increased half-life of RhoB induced by palmitoylation inhibition, which alters RhoB trafficking and increases its stability (Pérez-Sala et al., 2009). As RhoB and Arf6 colocalization was mainly observed in endocytic vesicles (Fig. 2, A and B), the increase of RhoB levels in the cytosol may have facilitated complex formation. Although Arf6 may recruit RhoB via interaction with the GCI residues, subsequent events, such as palmitoylation, may be needed to anchor the doubly lipidated RhoB at the membrane, thereby facilitating Arf6–RhoB complex formation at specific subcellular compartment. Altogether, the GCI of RhoB appears to be important for its interaction with Arf6 and for its retention in endosomes in the context of our study.

The crosstalk between Rac1-Arf6 and Rac1-RhoB plays critical roles in the regulation of cell shape and actin cytoskeleton remodeling. Arf6 colocalizes with Rac1 on endosomes, and Rac1-stimulated membrane ruffling requires Arf6 activity (Radhakrishna and Donaldson, 1997). In response to HGF, Arf6 KD attenuates recycling of Rac1-positive endosomes to the PM (Palamidessi et al., 2008). RhoB is also implicated in Rac1 trafficking toward the cell border and endosomal compartments (García-Weber and Millán, 2018). By modulating Rac1 and the RacGEF Tiam1 trafficking from endosome to the PM, RhoB regulates the disruption of intercellular junctions, cell protrusions, and actin stress fiber formation, thereby controlling cell migration and invasion

(Birukova et al., 2007). Our results revealed that Arf6 colocalizes and interacts with RhoB at the endosome. RhoB resides primarily at the PM when farnesylated (Wherlock et al., 2004), whereas geranylgeranylated RhoB is mainly localized to late endosomes (Wheeler and Ridley, 2004). Activation of Arf6 through nucleotide exchange triggers membrane recycling from endosome to the PM (Radhakrishna and Donaldson, 1997; Donaldson, 2003). In our model, RhoB mainly localized to the endosomes (Fig. 3 G). Therefore, we hypothesize that during its GTP/GDP cycling, Arf6 complexes with RhoB in the endosome, and the Arf6–RhoB complex may be required to regulate the intracellular trafficking of several signaling effectors, such as Rac1 or integrin β1, toward the PM to modulate Met/HGF-mediated cell motility.

Accordingly, the motile and invasive phenotype induced by the inhibition of RhoB is the result of increased Rac1-driven, actin-rich lamellipodial protrusions and the activation of the Akt1 and Rac1 pathways (Bousquet et al., 2009; Vega et al., 2012). Here, we found that the depletion of Arf6 or RhoB alters actin cytoskeleton and induces formation of rounded cells. This alteration of cell adhesion dynamics could be the consequence of a reduced cell attachment to several matrix proteins. In agreement with that proposition, a correlation between reduced cell adhesion associated with a defect in integrin-β1 recycling/distribution and enhanced migration has previously been reported in many models, such as in cells overexpressing Tiam1 (Minard et al., 2006; Vega et al., 2012). Therefore, we propose a model whereby the depletion of Arf6 promotes the loss of RhoB from endosomal membranes and lysosomal-dependent degradation of RhoB, leading to enhanced Rac1 signaling, reorganization of actin cytoskeleton, and cell migration. In agreement with this hypothesis, we found that Rac1 activity is strongly increased in RhoB- and Arf6-depleted cells in response to HGF stimulation (Fig. S3 H).

Recycling has emerged as a critical mechanism to spatiotemporally coordinate localized signaling complexes and actin dynamics and direct cell movement downstream of mitogenic stimuli and their receptors, such as Met (Palamidessi et al., 2008; Parachoniak et al., 2011; Ratcliffe et al., 2019). Our study demonstrates that Arf6–RhoB signaling plays an important role in governing Met RTK migratory responses. Our findings identify a novel regulatory mechanism for RhoB localization and stability by Arf6 and establish the strict requirement of Arf6 for RhoB-specific subcellular targeting to endosomes and, therefore, the regulation of membrane trafficking and cell motility.

Materials and methods

Cell culture and transfection
SKBr3, MDA-MB-231, and HeLa cells were maintained in DMEM containing 10% FBS. Transient transfections of HeLa cells were performed using Lipofectamine/Plus reagent (Invitrogen), and transfections of SKBr3 cells were performed using Lipofectamine 2000 (Invitrogen) or nucleofection (Amaxa), according to the manufacturers' instructions.

Antibodies and reagents
Commercially available antibodies were purchased as follows: anti-Arf6 (sc-7971), anti-RhoA (sc-418), anti-RhoB (sc-8048),

anti-RhoB (sc-180), anti-RhoC (12116), and anti-GST-B-14 (sc-138) were obtained from Santa Cruz Biotechnology; anti-Arf6 (AB77581) from Abcam; HA.11 from Berkeley; GFP from Roche; and anti-β-actin (AC-15) from Sigma-Aldrich. CAPTUREome S-Palmitoylated protein mini-Kit (K010-310) was from Badrilla, bafilomycin A1 (196000) was from Calbiochem, and 2-BP (21604-1G) was from Sigma-Aldrich. Arf6 siRNAs were custom designed within the 3′-untranslated region between nucleotides 1,813 and 1,837 (Thermo Fisher Scientific; 5′-CACAUCAUG CAUGAGUAGGAAUAUU-3′). AllStars Negative Control siRNA was purchased from Qiagen, and RhoB siRNA (sc-29472) was purchased from Santa Cruz Biotechnology. Control shRNA (RHS4080), Arf6 shRNA (RHS3979-2008001910), and RhoB shRNA (RHS3979-200801754) were purchased from Thermo Fisher Scientific. pcDNA3-EGFP (13031) was purchased from Addgene. RhoA-GFP and RhoB-GFP were obtained from Mark R. Philips (NYU Cancer Institute, New York, NY). TagRFP-T-RhoB was obtained from Michael W. Davidson (Florida State University, Tallahassee, FL). HA-RhoB, HA-RhoB-V14, and HA-RhoB-N19 were obtained from George C. Prendergast (Lankenau Institute for Medical Research, Wynnewood, PA). RhoB C193S was obtained from Dolores Pérez-Sala (Centro de Investigaciones Cientificas, Madrid, Spain). RhoA-mCherry was obtained from Guojun Sheng (RIKEN Center for Developmental Biology, Kobe, Japan). Arf6 WT and the Arf6 deletion mutants Arf6 28–175 and Arf6 73–175 were given by Kwok-Fai Lau (Chinese University of Hong Kong, Hong Kong, China). Arf6-mCherry, Arf6-GFP, Arf6-GFP Q67L, and Arf6-GFP T27N were obtained from Philippe Chavrier (Pierre and Marie Curie University, Paris, France). HA-Arf6, HA-Arf6-Q67L, and HA-Arf6-T27N were described in Lamorte and Park (2003). Myr-Flag-Arf6 was obtained from Sidney W. Whiteheart (Saha Cardiovascular Research Center, Lexington, KY; Choi et al., 2006). Arf6 WT as subcloned into p3XFLAG-CMV™ expression vector (Sigma-Aldrich), which contains an additional myristoylation site upstream of the three adjacent FLAG epitopes to increase the membrane localization of Arf6. The Myr-Flag-Arf6 constructs were subcloned into a GFP-vector plasmid using EcoRI and BamHI restriction sites. Actin-mCherry was obtained from Victor Small (Institute of Molecular Biotechnology, Vienna, Austria), and Paxillin-EGFP was obtained from A.R. Horwitz (University of Virginia, Charlottesville, VA). The chimeric protein Mito-Arf6-EGFP containing the mitochondrial sequence Su9 (amino acids 1–69; C-terminus) from ATPase subunit 9 of *Neurospora crassa* (Kondo-Okamoto et al., 2003) was obtained from Janet M. Shaw (University of Utah, Salt Lake City, UT) and subcloned using EcoRI and XhoI restriction sites to generate the chimeric protein.

Live-cell imaging
Cells were grown on collagen-coated glass coverslips (35 mm; Ibidi) for 48 h and stimulated for 20 min with 0.5 nM HGF (Genentech) or Alexa Fluor 555–conjugated HGF (HGF-555), unless otherwise specified. Images were collected on a motorized stage equipped with an inverted microscope, Axiovert 200 M (Carl Zeiss) with a 100× plan Apochromat NA 1.4 objective and an AxioCam HRM digital camera (Carl Zeiss). Cells were maintained within a chamber (Climabox, Carl Zeiss) with 5%

(vol/vol) CO_2 in air at 37°C. The microscope was driven by AxioVision LE software (Carl Zeiss). The motorized stage advanced to preprogrammed locations, and photographs were collected for 2 min at 4-s intervals for time-lapse imaging. For 3D cell migration, 6-well plates (Costar) were coated with 0.2% Geltrex (Reduced Growth Factor Basement Membrane Matrix) for 1 h at 37°C. MDA-MB-231 cells were suspended in DMEM, mixed with rat tail collagen (Roche), and plated on top of the Geltrex. Photographs were collected for 20 h at 10-min intervals for time-lapse imaging, at a frame rate of 29 fps. Routinely, 5×10^4 cells were embedded into 200 µl of 30–35% Geltrex. DMEM was added, and spheroid-like structures were allowed to form over 3 d at 37°C. The cells were stimulated with HGF (0.5 nM), and time-lapse imaging was performed as described above.

Scanning EM
Cells were stimulated with HGF (0.5 nM) and fixed with 4% formaldehyde overnight at 4°C. Preparations were then washed three times for 5 min in 0.2 M cacodylate buffer (pH 7.4) and rinsed with distilled water. Samples were dehydrated through a graded series (30–100%) of ethanol and dried with CO_2 in a Balzers CPD 030. Dried specimens were sputter-coated with palladium with a Bal-Tec MED 010 evaporator and were examined and photographed with a Hitashi S-3000N emission scanning electron microscope operating at 15 kV. Images were pseudocolored with Adobe Photoshop software.

Quantification of cell rear projections
The pictures from time-lapse microscopy were used to measure the size of cell rear projections from three independent experiments ($n = 400$ cells). Means of size were calculated using MetaMorph and Excel (Microsoft Office) software.

Quantification of stress fibers
The differences in stress fibers were quantified as previously described (Acharya et al., 2008). Briefly, ImageJ software (National Institutes of Health) was used to generate line profiles. A graphic depiction was then generated where the x axis represented the distance across the cell, the y axis represented the level of fluorescence, and each immunofluorescence intensity spike represented an individual stress fiber crossed by the line in ImageJ software. We randomly selected 20 cells and three regions in each cell for the quantification of 200 stress fibers.

Quantification of adhesion sites and FRAP
Stable adhesions were selected from the leading edge of migrating cells. Images of Paxillin-expressing cells ($n = 20$) were acquired every 4 s for 2 min. Background-corrected fluorescence intensity images were used to measure small adhesion sites and FA size and number (Zaoui et al., 2008). FRAP experiments were performed on a confocal microscope (LSM710; Carl Zeiss) with a 100× plan Apo 1.4 NA objective. For FAs, EGFP fluorescence (from 10 cells and 30 adhesions for stimulated cells; 20 cells and 40 adhesions for unstimulated cells) was eliminated by 30 bleach cycles at 100% intensity of the 488-nm argon laser. Recovery curves generated from photobleached areas of the same size and locations were sampled every 1 s for 2 min and corrected for

overall photobleaching, and then used to calculate percentage of fluorescence recovery by Zen LE software (Carl Zeiss).

Rho GTPase activity assay

The Rho GTPase activation assay was performed using the G-LISA RhoA, RhoB, and Rac1 absorbance-based activation assay (Cytoskeleton). Briefly, cells were grown on collagen-coated 6-well plates (Nunc), treated for 2 h with DMSO or 10 nM of bafilomycin A1 (Calbiochem), stimulated at different times with HGF (0.5 nM), and incubated at 37°C. Cells were then washed twice with ice-cold 1× PBS and resuspended in 65 µl of G-LISA lysis buffer. Protein lysates were transferred to ice-cold 1.5-ml centrifuge tubes and clarified by centrifuging at 10,000 rpm for 2 min. Protein concentrations were determined using the Bradford Protein Assay (Bio-Rad), and 1.0 mg/ml protein was used for the Rho GTPase activation assay as per the manufacturer's recommendations, with the exception of RhoB GTPase activity in which a RhoB-specific antibody (sc-8048; Santa Cruz Biotechnology) was substituted for the supplied RhoA antibody (Hall et al., 2008). A 1:50 dilution of the primary antibody and 1:250 dilution of the HRP-conjugated secondary antibody was sufficient to produce a RhoB-specific signal. After antibody and HRP reagent incubation, signals were detected on a Varioskan Flash Spectral Scanning Multimode reader at 490 nm (Thermo Fisher Scientific). Data analysis was performed using Excel. The activation levels of expressed Arf6 proteins were assayed as described previously (Jacquemet and Humphries, 2013). Briefly, 24 h after transfection, HeLa cells were lysed at 4°C in 1 ml of lysis buffer (1% Triton X-100, 50 mM Tris-HCl, pH 7.5, 150 mM NaCl, 10 mM MgCl$_2$, 0.5% deoxycholate, 0.1% SDS, 10% glycerol, 2 mM dithiothreitol, and protease inhibitors). Lysates were clarified by centrifugation at 13,000 rpm for 10 min and incubated with 0.5% BSA and 40 µg of GST-GGA3 bound to glutathione-Sepharose beads (Amersham Biosciences) for 40 min. The beads were washed three times with Arf6 washing buffer (50 mM Tris-HCl, pH 7.5, 100 mM NaCl, 2 mM MgCl$_2$, 1% NP-40, and 10% glycerol), and bound proteins were eluted in 30 µl of SDS sample buffer. The presence of Arf6-GTP was detected by immunoblotting using anti-HA antibody.

Immunoprecipitation and Western blot analysis

Cells were harvested in 1% Triton X-100 lysis buffer (150 mM NaCl, 20 mM Tris HCl, 1 mM EDTA, 1 mM EGTA, 1% Triton X-100, and 1% deoxycholate, at pH 7.4). All lysis buffers were supplemented with 1 mM PMSF, 1 mM sodium vanadate, 1 mM sodium fluoride, 10 µg/ml aprotinin, and 10 µg/ml leupeptin. Samples were resolved by SDS-PAGE and transferred to nitro-cellulose. Membranes were blocked with 5% BSA and probed as described with appropriate antibodies: anti-Arf6 (sc-7971), anti-RhoA (sc-418), anti-RhoB (sc-8048), anti-RhoC (12116), and GST.B-14 (Santa Cruz Biotechnology); HA 0.11 (Berkeley); GFP (Roche); and anti-β-actin (AC-15; Sigma-Aldrich). This was followed by incubation with HRP-conjugated secondary antibodies. All immunoblots were visualized by enhanced chemiluminescence (Amersham Biosciences). For immunoprecipitations, lysates were incubated with antibody at 4°C overnight with gentle rotation followed by 1-h incubation with protein A or G

Sepharose beads. Captured proteins were collected by washing three times in lysis buffers, eluted by boiling in SDS sample buffer, and processed as above for Western blotting.

In vitro binding assay

The GST-WT protein used for GST pull-down experiments included GST-RhoA (Cytoskeleton), GST-Arf6 (obtained from Gwyn W. Gould, University of Glasgow, Glasgow, Scotland), and GST-RhoB (obtained from Isabelle Lajoie-Mazenc, Faculté des sciences pharmaceutiques, Toulouse, France). His-Arf6 and His-RhoB were introduced into *Escherichia coli* BL21 (DE3) pLysS, and the fusion proteins were induced with 0.1–1 mM isopropyl-β-D-thiogalactopyranoside for 3–6 h. For binding assays, 2 µg of GST-tagged protein was incubated with 2 µg of His-tagged protein in lysis buffer (1% Triton X-100). Protein complexes were pulled down with G-Sepharose beads (GE Healthcare), washed three times with lysis buffer, and then subjected to Western blot analysis.

Pull-down assay for GTP-bound Rho GTPases

GST-proteins were loaded with GDP or GTPγS (Cytoskeleton) according to the manufacturer's instructions. Briefly, GTPγS was added to a final concentration of 0.2 mM, and GDP was added to a final concentration of 1 mM. The tubes were incubated for 1 h at 37°C before overnight incubation with 2 µg of His-Arf6 or His-RhoB produced by bacteria. The loading was stopped by adding MgCl$_2$ to a final concentration of 60 mM to each tube, which was then mixed and placed on ice until Western blot analysis. For Fig. 2 J, GST, GST-Arf6, GST-Arf6 28–175, and GST-Arf6 73–175 were transfected into HeLa cells. Protein lysates were then subjected to a GST pull-down and immunoblotted for endogenous RhoB.

Detection of palmitoylated RhoB by Acyl-RAC

Protein S-palmitoylation was assessed using CAPTUREome S-Palmitoylated protein assay by resin-assisted capture (acyl-RAC), according to manufacturer's instructions (K010-310; Ba-drilla). Briefly, 500 µl of blocking buffer (4 µl Thiol Blocking Reagent per 500 µl of buffer A) was added to 2 mg of protein. Samples were then vortexed for 5 s and incubated at 40°C for 4 h, with constant agitation. Three volumes (1.5 ml) of ice-cold acetone were added to each sample. Samples were vortexed for 5 s, and proteins were precipitated at –20°C for 20 min. The protein pellets were washed five times with ice-cold 70% acetone and air-dried. The pellets were redissolved in 300 µl of 1× binding buffer and centrifuged at 13,000 rpm for 1 min to remove any insoluble material. For thioester cleavage and resin capture, 50 µl of the resin slurry and 19 µl of Thioester Cleavage Reagent solution (previously prepared) were added to each sample. After 2.5-h incubation at room temperature with constant agitation, the samples were centrifuged for 1 min at 13,000 rpm and washed five times in 1 ml of 1× binding buffer. After removing the final wash, captured proteins were eluted using 50 µl of 2× Laemmli sample buffer and heated to 60°C for 10 min. Samples were resolved by SDS-PAGE and analyzed by immunoblotting using RhoB antibody (sc-8048) from Santa Cruz Biotechnology.

Immunofluorescence microscopy and quantification

Cells grown on collagen-coated coverslips were fixed in 4% formaldehyde at room temperature and permeabilized in 0.2% Triton X-100 before the addition of antibodies. The following antibodies were used for immunofluorescence: Met (AF276; R&D Systems); RhoB (sc-8048) and RhoB (sc-180; Santa Cruz Biotechnology; Fig. S1 D); Arf6 (AB77581; Abcam; Fig. S1 D); Paxillin (610051; BD Transduction Laboratories); and Flag (2368; Cell Signaling Technology). Secondary antibodies; Alexa Fluor 488, 546, and 633; and Phalloidin were obtained from Molecular Probes. Images were recorded with a scanning confocal microscope (LSM 510 Meta laser; Carl Zeiss) with a 100× plan Apo 1.4 NA objective and driven by Zen LE software. The degree of colocalization, expressed as the Pearson's correlation coefficient, was assessed by the colocalization analysis function of Imaris software (Bitplane). Results were logged into Excel for analysis. All values are means ± SEM from three independent experiments.

Statistics

All statistical analyses were performed using Excel. Graphed data represent the average values ± SEM from at least three independent experiments. Statistical significance was assessed using a two-tailed Student's t test. P values and the number of experiments used for quantification and statistical analysis are indicated in the corresponding figure legends. Data distribution was assumed to be normal, but this was not formally tested.

Online supplemental material

Fig. S1 shows the effect of RhoB down-regulation on the activation of Arf6 and cell morphology following HGF stimulation. Fig. S2 provides a specific relationship between Arf6 and RhoB. Fig. S3 describes the role of Arf6 and RhoB on the regulation of the actin stress fibers and FA dynamics. Video 1 shows the movement of MDA-MB-231 control cells cultured in 3D-Geltrex and stimulated with HGF (0.5 nM). Video 2 shows the movement of MDA-MB-231 cells cultured in 3D-Geltrex after Arf6 depletion and stimulated with HGF (0.5 nM).

References

Acharya, P.S., S. Majumdar, M. Jacob, J. Hayden, P. Mrass, W. Weninger, R.K. Assoian, and E. Puré. 2008. Fibroblast migration is mediated by CD44-dependent TGF beta activation. *J. Cell Sci.* 121:1393–1402. https://doi.org/10.1242/jcs.021683

Adamson, P., H.F. Paterson, and A. Hall. 1992. Intracellular localization of the P21rho proteins. *J. Cell Biol.* 119:617–627. https://doi.org/10.1083/jcb.119.3.617

Birukova, A.A., E. Alekseeva, A. Mikaelyan, and K.G. Birukov. 2007. HGF attenuates thrombin-induced endothelial permeability by Tiam1-mediated activation of the Rac pathway and by Tiam1/Rac-dependent inhibition of the Rho pathway. *FASEB J.* 21:2776–2786. https://doi.org/10.1096/fj.06-7660com

Boshans, R.L., S. Szanto, L. van Aelst, and C. D'Souza-Schorey. 2000. ADP-ribosylation factor 6 regulates actin cytoskeleton remodeling in coordination with Rac1 and RhoA. *Mol. Cell. Biol.* 20:3685–3694. https://doi.org/10.1128/MCB.20.10.3685-3694.2000

Bourne, H.R., D.A. Sanders, and F. McCormick. 1991. The GTPase superfamily: conserved structure and molecular mechanism. *Nature.* 349:117–127. https://doi.org/10.1038/349117a0

Bousquet, E., J. Mazières, M. Privat, V. Rizzati, A. Casanova, A. Ledoux, E. Mery, B. Couderc, G. Favre, and A. Pradines. 2009. Loss of RhoB expression promotes migration and invasion of human bronchial cells via activation of AKT1. *Cancer Res.* 69:6092–6099. https://doi.org/10.1158/0008-5472.CAN-08-4147

Chen, W., D. ten Berge, J. Brown, S. Ahn, L.A. Hu, W.E. Miller, M.G. Caron, L.S. Barak, R. Nusse, and R.J. Lefkowitz. 2003. Dishevelled 2 recruits beta-arrestin 2 to mediate Wnt5A-stimulated endocytosis of Frizzled 4. *Science.* 301:1391–1394. https://doi.org/10.1126/science.1082808

Chen, W., S. Niu, X. Ma, P. Zhang, Y. Gao, Y. Fan, H. Pang, H. Gong, D. Shen, L. Gu, et al. 2016. RhoB Acts as a Tumor Suppressor That Inhibits Malignancy of Clear Cell Renal Cell Carcinoma. *PLoS One.* 11:e0157599. https://doi.org/10.1371/journal.pone.0157599

Choi, W., Z.A. Karim, and S.W. Whiteheart. 2006. Arf6 plays an early role in platelet activation by collagen and convulxin. *Blood.* 107:3145–3152. https://doi.org/10.1182/blood-2005-09-3563

Cotton, M., P.L. Boulay, T. Houndolo, N. Vitale, J.A. Pitcher, and A. Claing. 2007. Endogenous ARF6 interacts with Rac1 upon angiotensin II stimulation to regulate membrane ruffling and cell migration. *Mol. Biol. Cell.* 18:501–511. https://doi.org/10.1091/mbc.e06-06-0567

D'Souza-Schorey, C., and P. Chavrier. 2006. ARF proteins: roles in membrane traffic and beyond. *Nat. Rev. Mol. Cell Biol.* 7:347–358. https://doi.org/10.1038/nrm1910

D'Souza-Schorey, C., and P.D. Stahl. 1995. Myristoylation is required for the intracellular localization and endocytic function of ARF6. *Exp. Cell Res.* 221:153–159. https://doi.org/10.1006/excr.1995.1362

D'Souza-Schorey, C., R.L. Boshans, M. McDonough, P.D. Stahl, and L. Van Aelst. 1997. A role for POR1, a Rac1-interacting protein, in ARF6-mediated cytoskeletal rearrangements. *EMBO J.* 16:5445–5454. https://doi.org/10.1093/emboj/16.17.5445

Donaldson, J.G. 2003. Multiple roles for Arf6: sorting, structuring, and signaling at the plasma membrane. *J. Biol. Chem.* 278:41573–41576. https://doi.org/10.1074/jbc.R300026200

Eades, G., B. Wolfson, Y. Zhang, Q. Li, Y. Yao, and Q. Zhou. 2015. lincRNA-RoR and miR-145 regulate invasion in triple-negative breast cancer via targeting ARF6. *Mol. Cancer Res.* 13:330–338. https://doi.org/10.1158/1541-7786.MCR-14-0251

Engel, M.E., P.K. Datta, and H.L. Moses. 1998. RhoB is stabilized by transforming growth factor beta and antagonizes transcriptional activation. *J. Biol. Chem.* 273:9921–9926. https://doi.org/10.1074/jbc.273.16.9921

Gampel, A., P.J. Parker, and H. Mellor. 1999. Regulation of epidermal growth factor receptor traffic by the small GTPase rhoB. *Curr. Biol.* 9:955–958. https://doi.org/10.1016/S0960-9822(99)80422-9

García-Weber, D., and J. Millán. 2018. Parallels between single cell migration and barrier formation: The case of RhoB and Rac1 trafficking. *Small GTPases.* 9:332–338. https://doi.org/10.1080/21541248.2016.1231655

Gherardi, E., W. Birchmeier, C. Birchmeier, and G. Vande Woude. 2012. Targeting MET in cancer: rationale and progress. *Nat. Rev. Cancer.* 12:89–103. https://doi.org/10.1038/nrc3205

Gillingham, A.K., and S. Munro. 2007. The small G proteins of the Arf family and their regulators. *Annu. Rev. Cell Dev. Biol.* 23:579–611. https://doi.org/10.1146/annurev.cellbio.23.090506.123209

Grossmann, A.H., J.H. Yoo, J. Clancy, L.K. Sorensen, A. Sedgwick, Z. Tong, K. Ostanin, A. Rogers, K.F. Grossmann, S.R. Tripp, et al. 2013. The small GTPase ARF6 stimulates β-catenin transcriptional activity during WNT5A-mediated melanoma invasion and metastasis. *Sci. Signal.* 6:ra14. https://doi.org/10.1126/scisignal.2003398

Grossmann, A.H., H. Zhao, N. Jenkins, W. Zhu, J.R. Richards, J.H. Yoo, J.M. Winter, B. Rich, T.M. Mleynek, D.Y. Li, and S.J. Odelberg. 2019. The small GTPase ARF6 regulates protein trafficking to control cellular function during development and in disease. *Small GTPases.* 10:1–12. https://doi.org/10.1080/21541248.2016.1259710

Hall, C.L., C.W. Dubyk, T.A. Riesenberger, D. Shein, E.T. Keller, and K.L. van Golen. 2008. Type I collagen receptor (alpha2beta1) signaling promotes prostate cancer invasion through RhoC GTPase. *Neoplasia.* 10:797–803. https://doi.org/10.1593/neo.08380

Hashimoto, S., S. Mikami, H. Sugino, A. Yoshikawa, A. Hashimoto, Y. Onodera, S. Furukawa, H. Handa, T. Oikawa, Y. Okada, et al. 2016. Lysophosphatidic acid activates Arf6 to promote the mesenchymal malignancy of renal cancer. *Nat. Commun.* 7:10656. https://doi.org/10.1038/ncomms10656

Hu, B., B. Shi, M.J. Jarzynka, J.J. Yiin, C. D'Souza-Schorey, and S.Y. Cheng. 2009. ADP-ribosylation factor 6 regulates glioma cell invasion through the IQ-domain GTPase-activating protein 1-Rac1-mediated pathway. *Cancer Res.* 69:794–801. https://doi.org/10.1158/0008-5472.CAN-08-2110

Huang, M., J.B. Duhadaway, G.C. Prendergast, and L.D. Laury-Kleintop. 2007. RhoB regulates PDGFR-beta trafficking and signaling in vascular smooth muscle cells. *Arterioscler. Thromb. Vasc. Biol.* 27:2597–2605. https://doi.org/10.1161/ATVBAHA.107.154211

Hunzicker-Dunn, M., V.V. Gurevich, J.E. Casanova, and S. Mukherjee. 2002. ARF6: a newly appreciated player in G protein-coupled receptor desensitization. *FEBS Lett.* 521:3–8. https://doi.org/10.1016/S0014-5793(02)02822-3

Jacquemet, G., and M.J. Humphries. 2013. IQGAP1 is a key node within the small GTPase network. *Small GTPases.* 4:199–207. https://doi.org/10.4161/sgtp.27451

Ju, J.A., and D.M. Gilkes. 2018. RhoB: Team Oncogene or Team Tumor Suppressor? *Genes (Basel).* 9:E67. https://doi.org/10.3390/genes9020067

Kazerounian, S., D. Gerald, M. Huang, Y.R. Chin, D. Udayakumar, N. Zheng, R.K. O'Donnell, C. Perruzzi, L. Mangiante, J. Pourat, et al. 2013. RhoB differentially controls Akt function in tumor cells and stromal endothelial cells during breast tumorigenesis. *Cancer Res.* 73:50–61. https://doi.org/10.1158/0008-5472.CAN-11-3055

Kondo-Okamoto, N., J.M. Shaw, and K. Okamoto. 2003. Mmm1p spans both the outer and inner mitochondrial membranes and contains distinct domains for targeting and foci formation. *J. Biol. Chem.* 278:48997–49005. https://doi.org/10.1074/jbc.M308436200

Lai, A.Z., J.V. Abella, and M. Park. 2009. Crosstalk in Met receptor oncogenesis. *Trends Cell Biol.* 19:542–551. https://doi.org/10.1016/j.tcb.2009.07.002

Lamorte, L., and M. Park. 2003. ARF1 and ARF6 are dispensable for Crk-dependent epithelial-mesenchymal-like transitions. *Anticancer Res.* 23:2085–2092.

Lamorte, L., I. Royal, M. Naujokas, and M. Park. 2002. Crk adapter proteins promote an epithelial-mesenchymal-like transition and are required for HGF-mediated cell spreading and breakdown of epithelial adherens junctions. *Mol. Biol. Cell.* 13:1449–1461. https://doi.org/10.1091/mbc.01-10-0477

Lee, G.Y., P.A. Kenny, E.H. Lee, and M.J. Bissell. 2007. Three-dimensional culture models of normal and malignant breast epithelial cells. *Nat. Methods.* 4:359–365. https://doi.org/10.1038/nmeth1015

Li, M., J. Wang, S.S. Ng, C.Y. Chan, M.L. He, F. Yu, L. Lai, C. Shi, Y. Chen, D.T. Yew, et al. 2009. Adenosine diphosphate-ribosylation factor 6 is required for epidermal growth factor-induced glioblastoma cell proliferation. *Cancer.* 115:4959–4972. https://doi.org/10.1002/cncr.24550

Li, R., C. Peng, X. Zhang, Y. Wu, S. Pan, and Y. Xiao. 2017. Roles of Arf6 in cancer cell invasion, metastasis and proliferation. *Life Sci.* 182:80–84. https://doi.org/10.1016/j.lfs.2017.06.008

Liu, A.X., N. Rane, J.P. Liu, and G.C. Prendergast. 2001. RhoB is dispensable for mouse development, but it modifies susceptibility to tumor formation as well as cell adhesion and growth factor signaling in transformed cells. *Mol. Cell. Biol.* 21:6906–6912. https://doi.org/10.1128/MCB.21.20.6906-6912.2001

Matsumoto, Y., H. Sakurai, Y. Kogashiwa, T. Kimura, Y. Matsumoto, T. Shionome, M. Asano, K. Saito, and N. Kohno. 2017. Inhibition of epithelial-mesenchymal transition by cetuximab via the EGFR-GEP100-Arf6-AMAP1 pathway in head and neck cancer. *Head Neck.* 39:476–485. https://doi.org/10.1002/hed.24626

Mazieres, J., T. Antonia, G. Daste, C. Muro-Cacho, D. Berchery, V. Tillement, A. Pradines, S. Sebti, and G. Favre. 2004. Loss of RhoB expression in human lung cancer progression. *Clin. Cancer Res.* 10:2742–2750. https://doi.org/10.1158/1078-0432.CCR-03-0149

Mellor, H., P. Flynn, C.D. Nobes, A. Hall, and P.J. Parker. 1998. PRK1 is targeted to endosomes by the small GTPase, RhoB. *J. Biol. Chem.* 273:4811–4814. https://doi.org/10.1074/jbc.273.9.4811

Meyer, N., A. Peyret-Lacombe, B. Canguilhem, C. Médale-Giamarchi, K. Mamouni, A. Cristini, S. Monferran, L. Lamant, T. Filleron, A. Pradines, et al. 2014. RhoB promotes cancer initiation by protecting keratinocytes from UVB-induced apoptosis but limits tumor aggressiveness. *J. Invest. Dermatol.* 134:203–212. https://doi.org/10.1038/jid.2013.278

Michaelson, D., J. Silletti, G. Murphy, P. D'Eustachio, M. Rush, and M.R. Philips. 2001. Differential localization of Rho GTPases in live cells: regulation by hypervariable regions and RhoGDI binding. *J. Cell Biol.* 152:111–126. https://doi.org/10.1083/jcb.152.1.111

Minard, M.E., L.M. Ellis, and G.E. Gallick. 2006. Tiam1 regulates cell adhesion, migration and apoptosis in colon tumor cells. *Clin. Exp. Metastasis.* 23:301–313. https://doi.org/10.1007/s10585-006-9040-z

Miura, Y., V. Ngo Thai Bich, M. Furuya, H. Hasegawa, S. Takahashi, N. Katagiri, T. Hongu, Y. Funakoshi, N. Ohbayashi, and Y. Kanaho. 2017. The small G protein Arf6 expressed in keratinocytes by HGF stimulation is a regulator for skin wound healing. *Sci. Rep.* 7:46649. https://doi.org/10.1038/srep46649

Morishige, M., S. Hashimoto, E. Ogawa, Y. Toda, H. Kotani, M. Hirose, S. Wei, A. Hashimoto, A. Yamada, H. Yano, et al. 2008. GEP100 links epidermal growth factor receptor signalling to Arf6 activation to induce breast cancer invasion. *Nat. Cell Biol.* 10:85–92. https://doi.org/10.1038/ncb1672

Muralidharan-Chari, V., H. Hoover, J. Clancy, J. Schweitzer, M.A. Suckow, V. Schroeder, F.J. Castellino, J.S. Schorey, and C. D'Souza-Schorey. 2009. ADP-ribosylation factor 6 regulates tumorigenic and invasive properties in vivo. *Cancer Res.* 69:2201–2209. https://doi.org/10.1158/0008-5472.CAN-08-1301

Osmani, N., F. Peglion, P. Chavrier, and S. Etienne-Manneville. 2010. Cdc42 localization and cell polarity depend on membrane traffic. *J. Cell Biol.* 191:1261–1269. https://doi.org/10.1083/jcb.201003091

Otsuka, Y., H. Sato, T. Oikawa, Y. Onodera, J.M. Nam, A. Hashimoto, K. Fukunaga, K.C. Hatanaka, Y. Hatanaka, Y. Matsuno, et al. 2016. High expression of EPB41L5, an integral component of the Arf6-driven mesenchymal program, correlates with poor prognosis of squamous cell carcinoma of the tongue. *Cell Commun. Signal.* 14:28. https://doi.org/10.1186/s12964-016-0151-0

Palacios, F., and C. D'Souza-Schorey. 2003. Modulation of Rac1 and ARF6 activation during epithelial cell scattering. *J. Biol. Chem.* 278:17395–17400. https://doi.org/10.1074/jbc.M300998200

Palacios, F., L. Price, J. Schweitzer, J.G. Collard, and C. D'Souza-Schorey. 2001. An essential role for ARF6-regulated membrane traffic in adherens junction turnover and epithelial cell migration. *EMBO J.* 20:4973–4986. https://doi.org/10.1093/emboj/20.17.4973

Palamidessi, A., E. Frittoli, M. Garré, M. Faretta, M. Mione, I. Testa, A. Diaspro, L. Lanzetti, G. Scita, and P.P. Di Fiore. 2008. Endocytic trafficking of Rac is required for the spatial restriction of signaling in cell migration. *Cell.* 134:135–147. https://doi.org/10.1016/j.cell.2008.05.034

Parachoniak, C.A., Y. Luo, J.V. Abella, J.H. Keen, and M. Park. 2011. GGA3 functions as a switch to promote Met receptor recycling, essential for sustained ERK and cell migration. *Dev. Cell.* 20:751–763. https://doi.org/10.1016/j.devcel.2011.05.007

Pellegrin, S., and H. Mellor. 2007. Actin stress fibres. *J. Cell Sci.* 120:3491–3499. https://doi.org/10.1242/jcs.018473

Pérez-Sala, D., P. Boya, I. Ramos, M. Herrera, and K. Stamatakis. 2009. The C-terminal sequence of RhoB directs protein degradation through an

endo-lysosomal pathway. *PLoS One.* 4:e8117. https://doi.org/10.1371/journal.pone.0008117

Radhakrishna, H., and J.G. Donaldson. 1997. ADP-ribosylation factor 6 regulates a novel plasma membrane recycling pathway. *J. Cell Biol.* 139:49–61. https://doi.org/10.1083/jcb.139.1.49

Ratcliffe, C.D.H., N. Siddiqui, P.P. Coelho, N. Laterreur, T.N. Cookey, N. Sonenberg, and M. Park. 2019. HGF-induced migration depends on the PI(3,4,5)P$_3$-binding microexon-spliced variant of the Arf6 exchange factor cytohesin-1. *J. Cell Biol.* 218:285–298. https://doi.org/10.1083/jcb.201804106

Ridley, A.J., M.A. Schwartz, K. Burridge, R.A. Firtel, M.H. Ginsberg, G. Borisy, J.T. Parsons, and A.R. Horwitz. 2003. Cell migration: integrating signals from front to back. *Science.* 302:1704–1709. https://doi.org/10.1126/science.1092053

Riento, K., and A.J. Ridley. 2003. Rocks: multifunctional kinases in cell behaviour. *Nat. Rev. Mol. Cell Biol.* 4:446–456. https://doi.org/10.1038/nrm1128

Robertson, D., H.F. Paterson, P. Adamson, A. Hall, and P. Monaghan. 1995. Ultrastructural localization of ras-related proteins using epitope-tagged plasmids. *J. Histochem. Cytochem.* 43:471–480. https://doi.org/10.1177/43.5.7537292

Rondanino, C., R. Rojas, W.G. Ruiz, E. Wang, R.P. Hughey, K.W. Dunn, and G. Apodaca. 2007. RhoB-dependent modulation of postendocytic traffic in polarized Madin-Darby canine kidney cells. *Traffic.* 8:932–949. https://doi.org/10.1111/j.1600-0854.2007.00575.x

Royal, I., N. Lamarche-Vane, L. Lamorte, K. Kaibuchi, and M. Park. 2000. Activation of cdc42, rac, PAK, and rho-kinase in response to hepatocyte growth factor differentially regulates epithelial cell colony spreading and dissociation. *Mol. Biol. Cell.* 11:1709–1725. https://doi.org/10.1091/mbc.11.5.1709

Sabe, H. 2003. Requirement for Arf6 in cell adhesion, migration, and cancer cell invasion. *J. Biochem.* 134:485–489. https://doi.org/10.1093/jb/mvg181

Spiering, D., and L. Hodgson. 2011. Dynamics of the Rho-family small GTPases in actin regulation and motility. *Cell Adhes. Migr.* 5:170–180. https://doi.org/10.4161/cam.5.2.14403

Takaishi, K., T. Sasaki, M. Kato, W. Yamochi, S. Kuroda, T. Nakamura, M. Takeichi, and Y. Takai. 1994. Involvement of Rho p21 small GTP-binding protein and its regulator in the HGF-induced cell motility. *Oncogene.* 9:273–279.

Tseliou, M., A. Al-Qahtani, S. Alarifi, S.H. Alkahtani, C. Stournaras, and G. Sourvinos. 2016. The Role of RhoA, RhoB and RhoC GTPases in Cell Morphology, Proliferation and Migration in Human Cytomegalovirus (HCMV) Infected Glioblastoma Cells. *Cell. Physiol. Biochem.* 38:94–109. https://doi.org/10.1159/000438612

Vega, F.M., and A.J. Ridley. 2018. The RhoB small GTPase in physiology and disease. *Small GTPases.* 9:384–393.

Vega, F.M., A. Colomba, N. Reymond, M. Thomas, and A.J. Ridley. 2012. RhoB regulates cell migration through altered focal adhesion dynamics. *Open Biol.* 2:120076. https://doi.org/10.1098/rsob.120076

Wang, D.A., and S.M. Sebti. 2005. Palmitoylated cysteine 192 is required for RhoB tumor-suppressive and apoptotic activities. *J. Biol. Chem.* 280:19243–19249. https://doi.org/10.1074/jbc.M411472200

Wheeler, A.P., and A.J. Ridley. 2004. Why three Rho proteins? RhoA, RhoB, RhoC, and cell motility. *Exp. Cell Res.* 301:43–49. https://doi.org/10.1016/j.yexcr.2004.08.012

Wheeler, A.P., and A.J. Ridley. 2007. RhoB affects macrophage adhesion, integrin expression and migration. *Exp. Cell Res.* 313:3505–3516. https://doi.org/10.1016/j.yexcr.2007.07.014

Wherlock, M., A. Gampel, C. Futter, and H. Mellor. 2004. Farnesyltransferase inhibitors disrupt EGF receptor traffic through modulation of the RhoB GTPase. *J. Cell Sci.* 117:3221–3231. https://doi.org/10.1242/jcs.01193

Yamauchi, Y., Y. Miura, and Y. Kanaho. 2017. Machineries regulating the activity of the small GTPase Arf6 in cancer cells are potential targets for developing innovative anti-cancer drugs. *Adv. Biol. Regul.* 63:115–121. https://doi.org/10.1016/j.jbior.2016.10.004

Yoo, J.H., D.S. Shi, A.H. Grossmann, L.K. Sorensen, Z. Tong, T.M. Mleynek, A. Rogers, W. Zhu, J.R. Richards, J.M. Winter, et al. 2016. ARF6 Is an Actionable Node that Orchestrates Oncogenic GNAQ Signaling in Uveal Melanoma. *Cancer Cell.* 29:889–904. https://doi.org/10.1016/j.ccell.2016.04.015

Zaoui, K., S. Honoré, D. Isnardon, D. Braguer, and A. Badache. 2008. Memo-RhoA-mDia1 signaling controls microtubules, the actin network, and adhesion site formation in migrating cells. *J. Cell Biol.* 183:401–408. https://doi.org/10.1083/jcb.200805107